Procedure for extending uv-limit of potential GMRT phase calibraters

Neeraj Gupta and Sanjay Bhatnagar
N.C.R.A., Pune
NCRA Technical Report

Abstract

The Ionosphere above the GMRT is relatively more turbulent compared to the northern latitudes, requiring the phase calibraters to be close to the target field in the sky. The VLA P-band calibrater list provides a list of compact sources which can be used as phase calibraters at low frequencies. Many of these sources are resolved at longer baselines or at lower frequencies (or both) and hence are not good phase calibraters for the GMRT. We therefore need a list of sources which cover the sky more uniformly for the GMRT and can be used as phase calibraters. However since unresolved sources are difficult to find at low frequencies and at GMRT resolutions, we need to build a database of image-plane models of compact sources. In conjunction with these image-plane models, even moderately resolved sources can be used as phase calibraters.

In this report, we describe a scheme we used to iteratively build an image-plane model of a Galactic plane calibrater ($J1829+487$), which is resolved at baselines $> 2K\lambda$ for GMRT at P-band. With this model, we show that the uv-range of this source is extended from 2Kλ to $\sim 25K\lambda$. This procedure can be used for other sources to build the above mentioned database of image-plane models. Since building this database involves a large amount of repetitive but useful work, we also explore the possibility of building a (semi-) automated software (pipeline?) which implements this scheme. A grading scheme to grade the derived image plane models and the effective range of the projected baseline lengths for which such a model is applicable is also proposed.

1 Introduction

A Radio interferometer samples the spatial coherence function of the radiation field as a function of the baseline (projected antenna separation measured in the units of wavelength). These measurements, called the Complex Visibilities (V_{ij}) can then be Fourier inverted under suitable assumptions to make the raw map of the corresponding radiation field. However, the observed visibilities (V_{ij}^{obs}) as measured by the interferometer needs to be *calibrated* to recover the true visibilities (V_{ij}^{true}). In the absence of any systematic baseline based offsets true visibilities are related to observed ones as

$$V_{ij}^{obs}(t) = g_{ij}(t)\ V_{ij}^{true}(t) + n_{ij} \tag{1}$$

where g_{ij} and n_{ij} are the baseline based complex gains and noise respectively. A very straightforward way to recover the true visibilities would be to look at a standard calibrater and determine the g_{ij}s i.e. baseline-based calibration. For various reasons antenna-based calibration is preferred over this method(see section 7.5 of reference 1).

In the antenna-based calibration scheme, $g_{ij}(t)$ is modeled as the product of two antenna-based complex gains:

$$g_{ij}(t) = g_i(t)\ g_j(t) = a_i(t)\ a_j(t)\ e^{i(\phi_i(t)-\phi_j(t))} \tag{2}$$

where $a_i(t)$ is the antenna based amplitude correction and $\phi_i(t)$ is the antenna based phase correction. These are traditionally determined from observations of an unresolved source. However at low frequencies many of the VLA calibrators show extended emission. Hence, they are not usable as the phase-calibrater in the usual scheme of calibration (see references 1 and 2). This imposes a limit on the uvrange[1] that can be used to compute the antenna based complex gains. Consequently, not all antennas can be calibrated using a resolved source. For the predominantly low frequency interferometers like the GMRT (Fig. 1), there is a serious dearth of phase calibrators since a significant fraction of the VLA calibrators are resolved at GMRT resolutions. The limit on the maximum baseline can however be relaxed if the structure of the source is known. Rest of the document describes a method of getting the source structure, starting from a point-source model and the corresponding uv(range)-limit.

2 Bootstrapping for antenna gains

For one of our observations with the GMRT at P-band, all good point source calibrators were either too weak or too far away in the sky from the target source. We therefore observed $J1829+487$, a moderately resolved source, as the phase calibrater. This source is resolved at baselines longer than $2K\lambda$ which means that we could use it to determine the phase offsets only for the Central square antennas. Therefore, to image the target source at full resolution, we needed an image-plane model for the calibrater. The antenna-based calibration allows one to solve for the antenna gains without using the full set of baseline data. In the following, we demonstrate a method which can be exploited to bootstrap and determine phase corrections for the whole array.

[1] uvrange specifies minimum and maximum projected baseline lengths (in units of the wavelength) to be used while solving for g_i's.

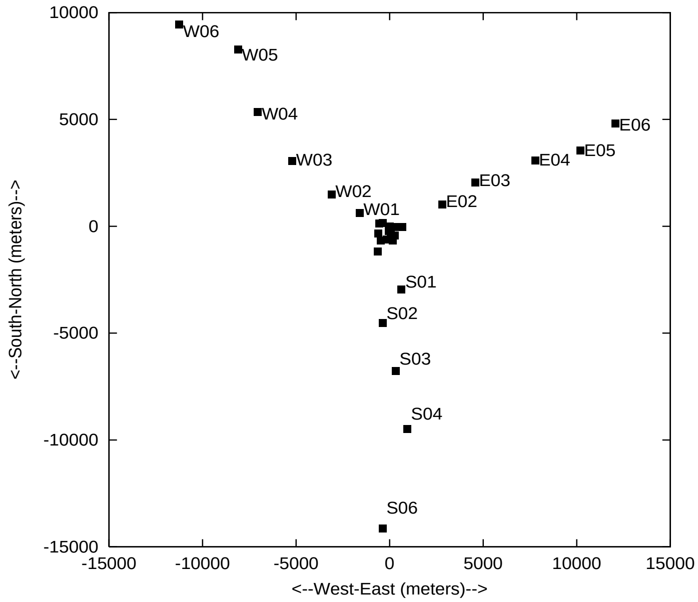

Figure 1: The figure shows all the 30 antennas of the GMRT with 14 of them clustered in the Central square and rest along the Western, Southern and Eastern arms.

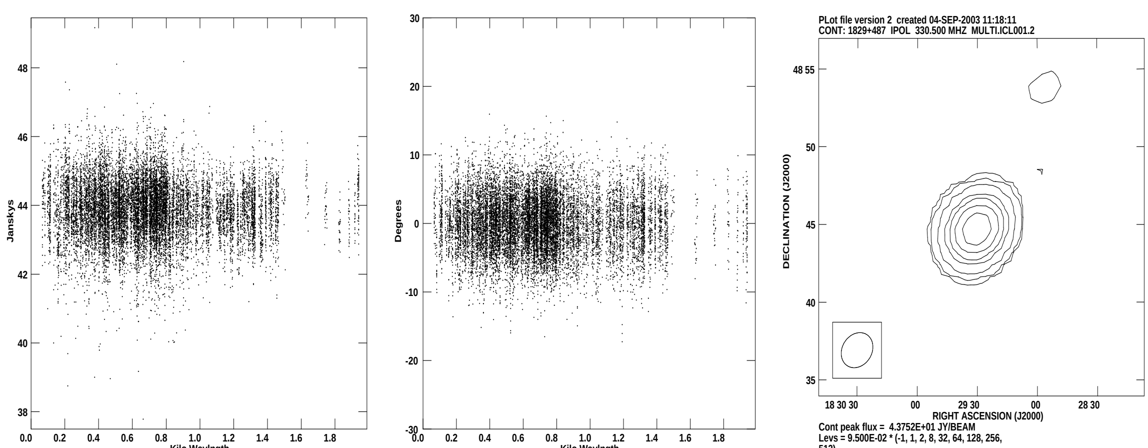

Figure 2: Figure showing calibrated visibilities for Central-square antennas only. The first and the second panel show the amplitude and phase respectively while the last panel shows the corresponding image for $J1829+487$. The source is unresolved till a baseline length of $2K\lambda$.

2.1 The method

Using the standard flux calibrater `3C48` and the AIPS tasks `SETJY`, `CALIB` (AIPS adverb `UVRAN` set to 0,2 for $J1829+487$) and `GETJY`, the P-band flux for $J1829+487$, using only the Central square antennas, was determined to be 43.89±0.84 Jy. All antennas other than the central square antennas were excluded at this step since not enough baselines $< 2K\lambda$ were found to provide good solutions for the gains of the arm antennas. Fig. 2 shows the calibrated visibilities (i.e. amplitude and phase) for the central square antennas. A map of $J1829+487$ was then obtained using the central square data only. This map, which would be used as the model at the next stage, was also Self-calibrated (see Fig. 2).

In the case with no `UVLIMIT` on $J1829+487$, one could have obtained gains for all the antennas. However since this is not the case, one needs to bootstrap starting from a uv-range of $2K\lambda$, to obtain the gains for the arm antennas. Following are the three possible routes for bootstrapping:

2.1.1 Route-a

Use the map obtained from the central square antennas as the model in `CALIB` and solve for all the antenna based gains (i.e. set `ANTENNA=0` and `UVRAN=0` or some high value say $10K\lambda$ in `CALIB`). Obviously, this is internally contradicting as one is using a point source model for a source which is actually extended (in this case for `UVRAN`$>$ 2Kλ). This limitation is indeed reflected in the extremely poor solutions obtained for the antenna gains in this case. Bitten by this, we instead move towards following two more conservative routes.

2.1.2 Route-b

In the task `CALIB` we increase the value of the AIPS adverb `UVRAN` to a moderate value of $4K\lambda$ and solve for the Central square antennas in addition to the nearest arm-antennas only (i.e., `W01, W02, E02` and `S01`). The data calibrated using the derived complex gains is shown in panel 2 of Fig. 3. At this stage, one may question the wisdom of choosing only `W01, W02, E02` and `S01` and increasing the value of `UVRAN` only to 4 not 3 or 6. Following are the justifications for this approach:

- One should definitely increase the uv-range by an amount which allows one to include some more antennas for solving since that is the aim of whole bootstrapping exercise. We noted that `UVRAN=3` does no good in this regard but `UVRAN=4` is good enough to have sufficient baselines for all the above mentioned antennas.
- Image model from the previous step with `UVRAN=2` should be a better model for this stage with `UVRAN=4` rather than, say for a value of 6 or 8 $K\lambda$.

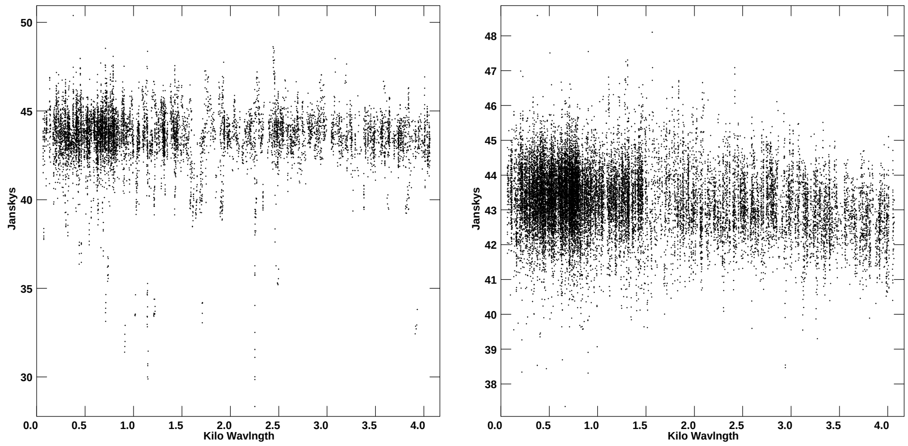

Figure 3: Comparison between Route-b and -c the bootstrapping. Right hand panel i.e. panel 1 and panel 2 show the data calibrated using the gains from Route-c and Route-b respectively.

- Breaking the bootstrapping into these small steps allows one to check intermediate results, i.e. it gives a better control on the whole process. This was important as we did not know apriori if the method would definitely work!

2.1.3 Route-c

Moderately increase the `UVRAN` to a value of, say $4K\lambda$ (refer to the arguments in Section 2.1.2) but apply no selection on the antennas to be used. The data so calibrated is shown in panel 1 of Fig. 3. Clearly, a number of poorly calibrated baselines are included. Arguably these baselines can be flagged and a better solution found. However, first of all, the data from these baselines is not intrinsically corrupted - it is just wrongly modeled. Secondly, as discussed in Section 3, from the point of view of automation of this process, flagging is not a good (or even correct!) option.

Thus, clearly, Route-b is the most appropriate. Therefore, solution for the gains of the Central square and the nearest arm-antennas `W01, W02, E02` and `S01` were found using the map obtained using baselines up to $2K\lambda$ (see the panel 3 of Fig. 2). The data so calibrated was imaged and the resulting image was also self-calibrated once. This image was then used as the image model in the next step. If this step was successful, then this image (Fig. 4) should produce a better model for the observed visibilities corrected for the antenna based offsets ($V_{ij}^{Cor} = V_{ij}^{obs}/g_i g_j^\star$). To check this we Fourier inverted the map to obtain the model visibilities (i.e. V_{ij}^{model}). If the model matches the data then $V_{ij}^{Cor}/V_{ij}^{model}$ should be close to unity, which is indeed true (see panel 2 of Fig. 4 for the normalized plot).

In the next iteration, `UVRAN` was increased to $6K\lambda$ and antennas `E03, S02, S03` and `W03` were also included. Input image model was the image from previous iteration (see Fig. 4). (see Fig. 5 for the map and the normalized plot. Map was also Self-calibrated).

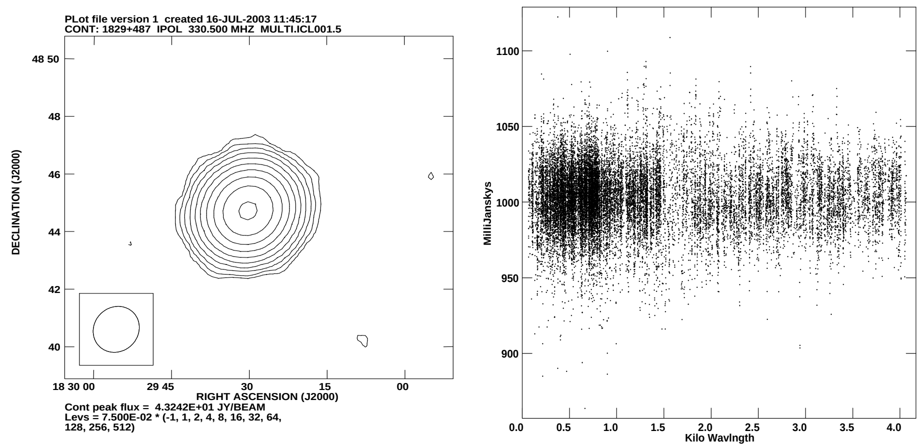

Figure 4: Map using $\mathrm{UV}_{max} = 4K\lambda$ i.e. Central square antenna along with W01,W02,E02 and S01 and the normalized visibilities i.e. $V_{ij}^{Cor}/V_{ij}^{model}$.

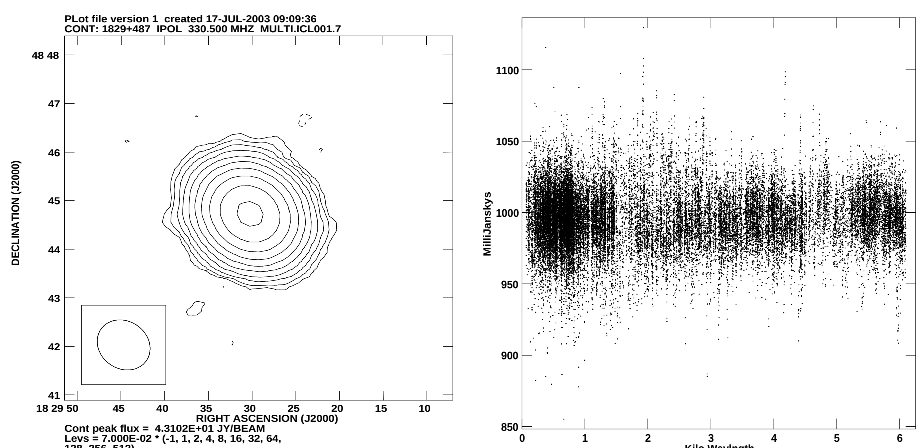

Figure 5: Map using $\mathrm{UV}_{max} = 6K\lambda$ i.e. E03, S02, S03 and W03 are also added and the normalized plot.

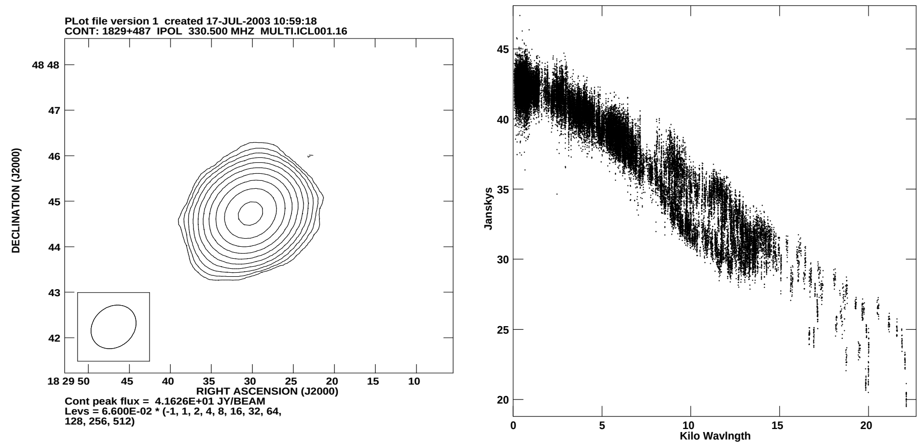

Figure 6: Map using $\mathrm{UV}_{max} = 8K\lambda$ with all the antennas and the full calibrated data.

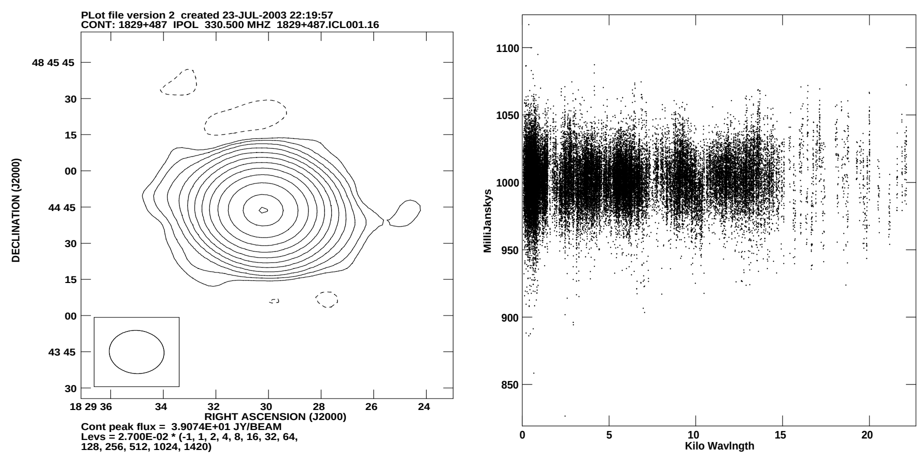

Figure 7: Map using all the data and the normalized plot.

In the final iteration, we also included `E04, E05, E06, W04, W05, S04, W06` and `S06` (i.e. the entire array). Again, as before, the input model image was the image from the previous iteration (the image in Fig. 6) and `UVRAN` increased to $8K\lambda$. Obviously, the gains so obtained should be applicable to all the visibilities (i.e. `UVRAN=0`). Panel 2 in the Fig. 6 shows the calibrated amplitude for the whole data. Again, if the method was successful, then $V_{ij}^{Cor}/V_{ij}^{model}$ should be close to unity. Fig. 7 shows that this is indeed true. Fig. 7 also shows the final image at full GMRT resolution.

3 Suggested future work

The procedure described in the previous section to make an image-plane model of a moderately resolved source such that $V_{ij}^{Cor}/V_{ij}^{model} \sim 1.0$ can be used to increase the effective uv-range of a number of calibraters in the VLA Calibrater list. The procedure can be summarized as:

1. Flag the data for dead/bad antennas and RFI (if any).
2. Set the uv-range to that given in the VLA Calibrater list.
3. Select a set of antennas, all of which satisfy at least one amplitude closure relation within the prescribed uv-range.
4. Self-calibrate this data using the uv-range. This will provide the complex antenna based gains (g_i°) for primary phase calibration for most of the antennas included in this uv-range.
5. Calibrate the data using g_i°, and make a deconvolved image (I^M) of the source using all the baselines which were calibrated in the previous step.
6. Decide the set of antennas to be used in the next step and the uv-range increment ΔB (see Section 3.3.1).
7. Use I^M as the model image and increase the uv-range by ΔB. Goto step 3.
8. Iterate till the uv-range includes the entire array and the uv-plot is constant for the entire uv-range ($V_{ij}^{Cor}/V_{ij}^{model} \sim 1.0$).

3.1 Can the process be automated?

Given that the procedure described in Section 2 can be tedious, repetitive and hence boring, it is useful to ask the question: Can this process be automated? The goal of automation is however not to eliminate the most 'intelligent' element in the chain - a human being. The goal is to significantly reduce the amount of data to a level where it is not too cumbersome for a human (or a co-operating set of humans!) to examine.

In what follows, we discuss each of the above steps in detail with the goal of exploring which of these steps can be automated.

3.2 Flagging

This is a crucial step, in which all RFI affected or otherwise corrupted data is flagged. The three major sources of data corruption are (1) RFI, (2) loss of signal from an antenna (referred to as 'dead antenna'), and (3) correlator problem.

The GMRT correlator naturally generates the time-frequency plane data for each baseline with up to 256 frequency channels . As shown in the work on auto-flagging (reference 3), this can be effectively used to remove outlier visibility points by examining the time-frequency plane data from cross- and self-correlations. Except a threshold setting, this flagger is reasonably automatic and robust. A program for this already exists and is in use on the GMRT data by various users of the telescope. Note that the threshold setting is easiest for an unresolved or moderately resolved source. Since all the sources we will use will be in this category, it is reasonable to assume that a large amount of flagging of type (1) and (2) above can be automated.

Experience shows that it is possible to identify data corrupted due to correlator problems and/or inordinately high T_{sys} at a few antennas using the robust algorithm (see reference 2). Again, this works best for unresolved or moderately resolved sources, which will be the case for all our sources.

It appears therefore that it is possible to implement a reasonably automated procedure for flagging corrupted data.

3.3 Calibration

Calibration essentially involves solving Eq. 1 for g_is. This can be done using a non-linear least square minimization algorithm. Since the right hand side of Eq. 1 in the bootstrapping scheme involves the model visibilities V_{ij}^{model} (which in turn are equal to Fourier transform of $B \star I^M$ where B is the PSF), solving Eq. 1 needs the model image. In the case of an unresolved source, V_{ij}^{model} is trivial. We refer to the algorithm used to solve Eq. 1 for an unresolved source as `antsol` (see reference 2). A robust implementation of `antsol` is implemented in the program `rantsol` and in practice has proved to be robust to the presence of bad/corrupted data and have been regularly used to automate various tasks (e.g. GMRT phased array mode, beam shape measurements, polarization purity estimates, baseline measurements, etc.). The program `calibbp` uses the `rantsol` algorithm to calibrate LTA data in time and frequency using an unresolved source.

It is easy to modify these programs to work for resolved sources by accepting a model image. With that modification, it appears that the step of calibration can also be reasonably automated.

3.3.1 UV-range

Two important parameters to determine for deriving antenna based complex gains in each cycle will be the values of ΔB and the antennas to be used. Including all baselines which fall within the selected uv-range in the uv-plane will certainly not be wise. This may result into an under-determined set of equations (i.e, may include antennas, the complex gains for which cannot be solved for). Rigorously speaking, visibilities from a set of antennas, each one of which satisfies at least one amplitude closure relation, constitute a solvable set of equations. This criteria can be used to determine the set of antennas to be used for a given uv-range.

ΔB can be determined by demanding that the uv-range at each iteration be increased by an amount which includes N more antennas than used in the previous iteration, all of which satisfy C amplitude closure relations. The values of N and C can be empirically determined. C will be function of the signal-to-noise (SNR) ratio in the data. The antenna based calibration process essentially determines a consistent set of antenna gains by averaging all the available closure relations. More closure relations reduces the error budget on the solutions. For high SNR data (which will be case for most of our observations), the process is expected to be weakly dependent on C. N can be determined by some heuristic argument (for moderately resolved sources, the convergence of the process will only weakly depend on this too).

3.4 Imaging

This step, particularly for unresolved or moderately resolved sources is easily automated. The three major operations needed for this step are (1) gridding/de-gridding the visibility data onto a regular grid, (2) Fourier transforming the gridded visibilities and the weights to form the Dirty Image and the PSF, and (3) deconvolve the Dirty Image using one of the standard deconvolution algorithms. Given a PSF, a minimum flux limit or the maximum number of iterations, and an image-plane window encompassing the compact source of interest, this step is already automated using the current deconvolution algorithms. High dynamic range and fidelity images can be made even more easily using the more modern algorithms (e.g. scale sensitive deconvolution algorithms).

Programs already exists with the authors which implements the deconvolution algorithm and can be easily modified to accept the GMRT native data recording format. It is therefore reasonable to assume that this step can be certainly automated.

3.5 Test of convergence

Step 7 in the above scheme is another crucial step where we determine if the process has converged. The final product of these iterations will be the model image and the corresponding normalized visibilities ($X_{ij} = V_{ij}^{Cor}/V_{ij}^{model}$). The Goodness-of-fit of a straight line to X_{ij} as a function of uv-distance $r = \sqrt{u^2+v^2}$ can be used to detect convergence. E.g. a possible measure of convergence can be $\chi^2 = \sum_{ij} |X_{ij}(r) - (m * r + F)|^2$ where m and F should be close to 0.0 and 1.0 and $\sqrt{\chi^2}$ should be equal to the RMS noise respectively. All the three numbers together will probably provide a robust measure of convergence. A gridded version of X_{ij}, which is smoothed by the gridding convolution function, is probably more appropriate for this test.

Perhaps, a more fundamental test of convergence is to check the number of closure relations (both amplitude and phase closure) that are satisfied to within the noise level. This can be checked by computing all the possible closure relations from $V^{obs}/g_i g_j^{\star}$.

4 Grading the Image Plane models

Final goal is to construct a data-base of image plane models which is readily available to the users. An objective grading of these models would allow observers to make quick decisions/choices without worrying about the details of the data-processing done to obtain the model for a given calibrator. We propose that the image plane models be classified into I+ and I- categories. Former corresponds to the image plane models that were obtained via calibrating the visibility data using some standard VLA calibrator. However, this may not always be possible, especially at the low frequencies. For example, for $J1829+487$ there is no nearby (not within 20°) compact P-band calibrator. In such cases, bootstrapping is the only way and consistency checks have to come from the analysis itself! As mentioned in the last section, one way to ascertain that bootstrapping has worked or not is to check the number of closure relations that are satisfied within the noise level. The image plane models so obtained can be graded as I-.

Another simpler way to check whether the bootstrapping worked or not is to look at the gains of the antennas common in two successive iterations of the bootstrapping process. E.g., lets say that the gains for say M antennas have been determined correctly in an iteration. Any significant change in the gains of these antennas in the next iteration would mean that at least one of the following two things is happening: (1) one of the new antennas included in the current iteration is really bad - i.e. gives high closure errors and hence corrupts the earlier solutions, or (2) the process is pushing the source structure based information into the antenna based gains and that is a serious problem. For $J1829+487$, we checked for such a consistency at each iteration. Satisfied with this, the image plane model for $J1829+487$ is marked as I- and can be used as an input model for solving for antenna gains in the future observations.

5 Conclusions

From the above analysis, we conclude that the entire processes of flagging, imaging and calibration, at least for compact sources, can be automated and the various parameters be tweaked to keep the chain of operations robust.

The scientific benefits of an automated and robust pipe-line are obvious. Hence we feel that it is worthwhile to make an effort to implement this automation as a software (single program or, probably more appropriately, a pipe-line consisting of a chain of otherwise independent programs).

The longer term benefit of this approach that we foresee are two:

1. The project of automating the flagging-calibrating-imaging operations, while will be immediately useful for a large project to build GMRT calibrater list, it will also be a good first step towards automating these operations possibly even for more complex sources.

2. Most other modern observatories are actively pursuing programs for as much automation in data processing as possible. These efforts are motivated by relatively large amount of data these new telescopes will generate as well as by the fact the man-made RFI environment, particularly at lower frequencies, is only going to deteriorate. Besides keeping the software and data analysis practices at NCRA modern, this also opens up another obviously useful possibility: that of quasi on-line imaging (at least for quick-look purposes). The structure of GMRT on-line control, data acquisition and off-line software systems is well suited for this work.

6 References

1. Chapter 5 of Synthesis Imaging in Radio Astronomy II; Eds. Taylor G. B., Carill C. L., and Perley R. A.; ASP Conference Series, Vol. 180

2. Bhatnagar S., Computation of Antenna Dependent Complex Gains, NCRA-TIFR Int.Tech.Report, Jan 1999, R00172

3. Urvashi R. V., A report on (1) Automatic RFI Identification and Flagging, (2) Numerical simulations for Solutions of Complex Antenna gains, NCRA-TIFR, June 2002, 1997B5A7169